pH-Dependent Structural Changes in the Active Site of *p*-Hydroxybenzoate Hydroxylase Point to the Importance of Proton and Water Movements during Catalysis[†,‡]

Domenico L. Gatti,[*,§] Barrie Entsch,[||] David P. Ballou,[§] and Martha L. Ludwig[§]

Department of Biological Chemistry and Biophysics Research Division, University of Michigan, Ann Arbor, Michigan 48109, and Department of Biochemistry, Microbiology and Nutrition, University of New England, Armidale, New South Wales 2351, Australia

Received June 14, 1995; Revised Manuscript Received October 24, 1995[⊗]

ABSTRACT: Deprotonation of *p*-hydroxybenzoate to the phenolate and reprotonation of the hydroxylated dienone intermediate to form the product are essential steps in the reaction catalyzed by *p*-hydroxybenzoate hydroxylase (PHBH). The mechanism by which protons are transferred in these reactions is not obvious, because the substrate bound in the active site is isolated from solvent. Structure analyses of wild-type and mutant PHBH, with bound *p*-hydroxybenzoate or *p*-aminobenzoate, reveal a chain of proton donors and acceptors (the hydroxyl groups of Tyr201 and Tyr385, and two water molecules) that can connect the substrate 4-OH to His72, a surface residue. This chain could provide a pathway for proton transfer to and from the substrate. Using various combinations of pH and substrates, we show that in crystalline PHBH ionizable groups in the chain may rotate and change hydrogen-bond orientation. Molecular dynamics simulations have been used to predict the preferred orientation of hydrogen bonds in the chain as a function of the ionization states of substrate and His72. The calculations suggest that changes in the ionization state of the substrate could be associated with changes in orientation of the hydrogen bonds in the chain. Transfer of water between the chain of proton donors and the solvent also appears to be an essential part of the mechanism that provides reversible transfer of protons during the hydroxylation reaction.

p-Hydroxybenzoate hydroxylase (PHBH)[1] (EC 1.14.13.2) catalyzes the monooxygenation of *p*-hydroxybenzoate (*p*-OHB) to form 3,4-dihydroxybenzoate. This reaction proceeds in two stages (Entsch *et al.*, 1976; Entsch & Ballou, 1989) (Scheme 1). In the first half-reaction, *p*-OHB and NADPH bind to the enzyme and NADPH reduces the FAD cofactor. In the ensuing oxidative reactions, reduced flavin reacts with oxygen to form flavin C(4a) hydroperoxide, and the distal oxygen of the hydroperoxide is transferred to position 3 of the substrate. As expected from the complexity of these reactions, conformational changes in the enzyme play an important role in the catalytic mechanism. We and others (Lah *et al.*, 1994a; Schreuder *et al.*, 1994; Gatti *et al.*, 1994) have shown that the flavin cofactor can occupy two different positions in the active site of the enzyme. In the "open" conformation the flavin ring has considerable exposure to solvent and a channel is formed that connects the bulk solvent to the active site. In the "closed" conformation, the substrate is buried inside the enzyme and the flavin ring occupies a position that isolates the C(4a) hydroperoxide group from solvent, thereby inhibiting the elimination of hydrogen peroxide and the uncoupling of NADPH consumption from substrate hydroxylation (Entsch *et al.*, 1991; Palfey, 1993).

Hydroxylation of *p*-OHB is expected to proceed through at least three steps (Entsch *et al.*, 1976). First, deprotonation of the 4-hydroxyl places a negative charge on the substrate O(4), which is delocalized on C(3) and C(5) (Scheme 2a). This delocalization, which should increase the reactivity of C(3) toward the electrophilic flavin hydroperoxide, has been inferred from molecular orbital calculations (Vervoort *et al.*, 1992). On the reaction coordinate, formation of the substrate phenolate is close to the postulated nonaromatic dienone intermediate (Scheme 2b). Formation of product (Scheme 2c) would then require tautomerization of the dienone with loss of one proton from C(3) and reprotonation of O(4).

The reaction mechanism outlined in Scheme 2 invokes changes in the protonation state of the substrate and of the reaction intermediates during turnover. Several studies have analyzed the pH dependence of the overall reaction and of the individual reductive and oxidative steps using both reactive substrates (*p*-hydroxybenzoate, *p*-aminobenzoate, 2,4-dihydroxybenzoate) and a nonsubstrate effector (6-hydroxynicotinate) (Shoun *et al.*, 1974, Shoun *et al.*, 1979; van Berkel & Müller, 1989; Wessiak *et al.*, 1984). It was observed that in the presence of *p*-OHB as substrate, the kinetic parameters of the reductive and oxidative half-reactions show variation in the pH range 6.5−9.5 (see also Table 2 in the Results and Discussion section) with a broad optimum around pH 8.0. However, observations of slow exchange of D_2O for H_2O in the active site (Palfey, 1993), and the evidence of physical insulation of the substrate from solvent, derived from the high-resolution structures of the

* To whom correspondence should be addressed.

† This work was supported by grants from NIH (GM 16429 to M.L.L. and GM 20877 to D.P.B.) and the Australian Research Council (to B.E.).

§ University of Michigan.

|| University of New England.

‡ Coordinates described in Table 1 have been deposited in the Brookhaven Protein Data Bank (ID codes 1IUS, 1IUT, 1IUU, 1IUV, 1IUW, 1IUX).

⊗ Abstract published in *Advance ACS Abstracts,* January 1, 1996.

[1] Abbreviations: PHBH, *p*-hydroxybenzoate hydroxylase; *p*-OHB, *p*-hydroxybenzoate; *p*-ABA, *p*-aminobenzoate; RMS, root mean square; SA, simulated annealing.

0006-2960/96/0435-567$12.00/0

Scheme 1: The Catalytic Cycle of PHBH[a]

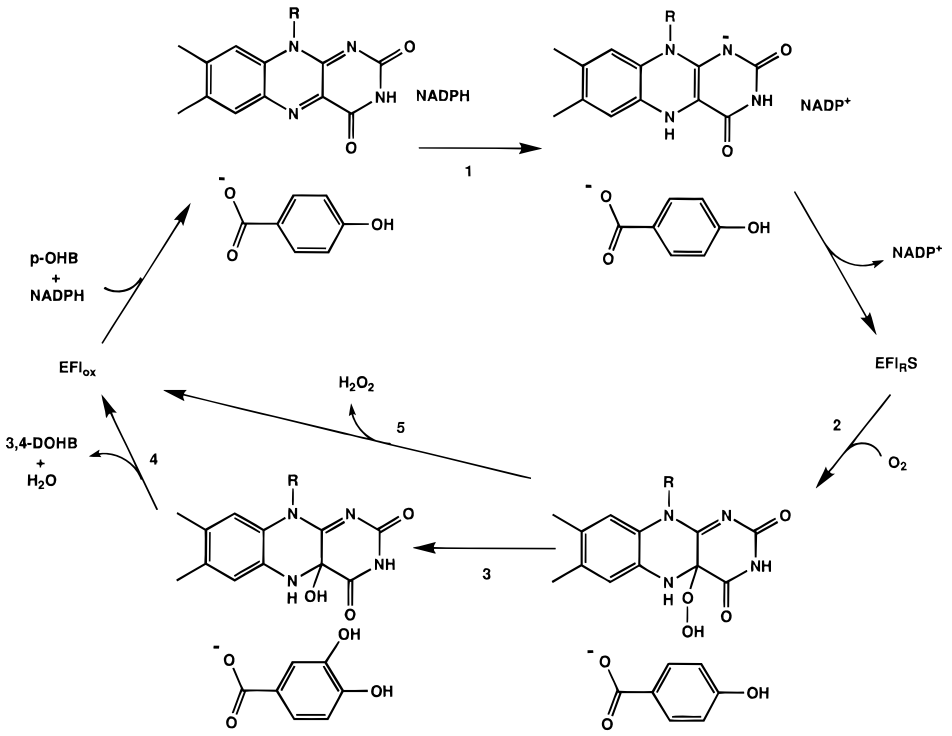

[a] The numbers near the arrows refer to reaction steps determined by stopped-flow kinetic analysis (Entsch *et al.*, 1976): (1) reduction of the flavin in the presence of substrate; (2) formation of the 4(a)-flavin hydroperoxide species; (3) substrate hydroxylation (this step is examined in more detail in Scheme 2); (4) release of the product 3,4-dihydroxybenzoate and dehydration of the flavin 4(a)-hydroxide; (5) uncoupling of NADPH oxidation from product formation with release of hydrogen peroxide. EFl_{ox}, enzyme with oxidized flavin. EFl_RS, enzyme with reduced flavin and *p*-OHB bound.

Scheme 2: Postulated Mechanism of Hydroxylation[a]

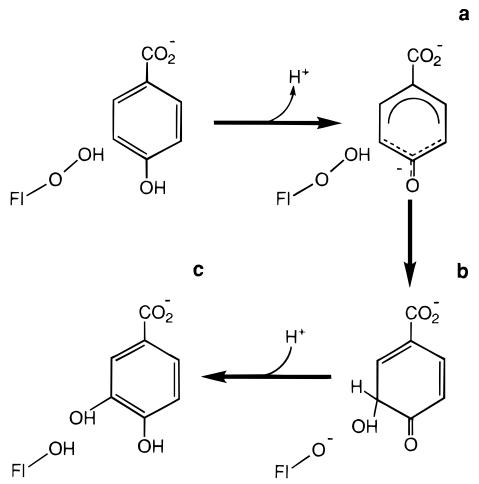

[a] The flavin hydroperoxide (Fl-O-OH), hydroxide (Fl-OH) and hydroxide anion (Fl-O^-) are shown on the left of the substrate, product, and reaction intermediate respectively. The steps where the substrate O(4) undergoes protonation/deprotonation are indicated by the arrows and proton symbols.

p-OHB−enzyme complex in both the oxidized (Schreuder *et al.*, 1988) and the reduced state of the flavin (Schreuder *et al.*, 1992), support the view that during turnover the chemical species involved in catalysis are not in rapid protonic equilibrium with solvent. This suggests that the protein may participate in the proton transfer events.

Mutational analyses of PHBH from *Pseudomonas fluorescens* (Eschrich *et al.*, 1993) and *Pseudomonas aeruginosa* (Entsch *et al.*, 1991; Lah *et al.*, 1994b) have pointed out the importance of Tyr201 and Tyr385 for optimal activation of the substrate. However, the mechanistic details of this activation are still unclear. Elucidation of the structures of additional intermediates, in particular those incorporating oxygenated forms of the flavin (Entsch *et al.*, 1976; Entsch & Ballou, 1989; Schreuder *et al.*, 1990), would therefore be of extreme interest. Unfortunately the half-lives of these species preclude structure analyses that utilize routine single-wavelength X-ray data acquisition. However, the changes occurring in the crystalline enzyme upon protonation/deprotonation of the substrate or in the presence of a substrate analog may partially mimic intermediate states of the enzyme. Thus, for instance, the lower pK_a of the bound as compared to the free *p*-OHB (Entsch *et al.*, 1991) might be an expression of the enzyme affinity for a deprotonated transition state and/or intermediate in the reaction of hydroxylation (Scheme 2). This idea has prompted us to study the stable states of the crystalline enzyme at different pH values in the presence of *p*-hydroxybenzoate (*p*-OHB) and in the presence of *p*-aminobenzoate (*p*-ABA).

MATERIALS AND METHODS

Crystals, Data Collection, and Structure Refinement. PHBH from *P. aeruginosa* was purified according to the procedure described by Palfey *et al.* (1994). Crystals were grown at pH 7.4 in the presence of substrate (*p*-OHB or *p*-ABA) by free interface diffusion in sealed melting-point capillaries of 1.3-mm diameter as described for the *P. fluorescens* enzyme by van der Laan *et al.* (1989): 5 μL of a solution containing 10 mg/mL PHBH in 0.1 M potassium phosphate (pH 7.4), 2 mM *p*-OHB or 4 mM *p*-ABA, 0.004 mM FAD, and 0.2 mM glutathione was layered inside an ice-cold melting-point capillary on top of 5 μL of 71% saturated ammonium sulfate in 0.1 M potassium phosphate

Table 1: Data Sets and Crystallographic Refinements[a]

	p-OHB			*p*-ABA		
	pH 5.0	pH 7.4	pH 9.4	pH 5.0	pH 7.4	pH 9.4
a axis (Å)	71.65	71.79	71.73	71.71	71.73	71.89
b axis (Å)	146.43	146.59	146.37	146.57	146.49	146.54
c axis (Å)	88.77	88.12	88.05	88.39	87.96	87.94
resolution (Å)	15−2.5	15−2.0	15−2.0	15−2.2	15−2.0	15−2.0
unique reflcns	16343	31420	31069	23957	31490	31276
completeness (%)	99.31	99.14	98.3	99.9	99.6	98.73
⟨redundancy⟩	6.32	11.6−3.5	7.58	8.34	8.74	8.25
$\langle I/\sigma I\rangle$	9.0	7.95	7.8	7.0	11.1	8.91
$\langle I/\sigma I\rangle$ (HighRes)[b]	2.21	3.10	1.95	2.01	2.94	2.08
R_{sym}[c]	0.097	0.09−0.04	0.100	0.113	0.101	0.112
R_{sym} (HighRes)[b]	0.310	0.284	0.295	0.302	0.244	0.336
R[d]	0.170	0.170	0.173	0.166	0.166	0.176
solvents	145	231	190	210	236	222
RMS coord. error[e] (Å)	0.298	0.202	0.216	0.249	0.187	0.225
RMS deviations[f]						
bond length (Å)	0.011	0.009	0.01	0.01	0.01	0.01
angles (deg)	1.667	1.551	1.582	1.642	1.578	1.577
dihedrals (deg)	23.98	24.0	24.03	24.04	24.21	24.20
impropers (deg)	1.472	1.332	1.384	1.447	1.343	1.369

[a] Data sets were collected at 22 °C with a dual multiwire area detector (Area Detector Systems, San Diego, CA). Intensity data for the *p*-OHB complex at pH 7.4 were obtained by merging a data set collected with the multiwire area detector (first number in the row for the values of redundancy and R_{sym}) with a data set collected with a single-image plate area detector (MAR Industries) (second number in the row for the values of redundancy and R_{sym}). $R_{merge} = \Sigma(h)\Sigma(j = 1, ..., N)\ |I(h) - I(h,j)|/\Sigma(h)\ NI(h)$. The R_{merge} for the merged data set was 0.079. [b] Highest resolution shell of 0.15-Å width. [c] $R_{sym} = \Sigma(h)\Sigma(i)\ |I(h,i) - \langle I(h)\rangle|/\Sigma(h)\Sigma(i)\ I(h,i)$ [$\langle I(h)\rangle$ = mean intensity of symmetry equivalent reflections (h)]. [d] $R = \Sigma(h)\ ||F_o(h)| - k|F_c(h)||/\Sigma(h)\ |F_o(h)|$. [e] RMS coordinate error was calculated using the Sigmaa program (Read, 1986) as implemented in the CCP4 (Collaborative Computational Project Number 4, 1994) suite of programs for X-ray crystallography. [f] RMS deviations from ideality for bonds and angles were calculated from the refined coordinates using X-PLOR (Brunger, 1992).

(pH 7.4). After heat-sealing, the capillaries were placed inside an incubator initially at 4 °C and the temperature was slowly raised to 23 °C over a period of 2 weeks. The capillaries were left undisturbed in the incubator at this final temperature for an additional 2 months. The holding solutions were 0.1 M in buffer (potassium 2-[*N*-morpholino]-ethanesulfonate at pH 5.0; potassium phosphate, at pH 7.4; Bis-tris propane sulfate at pH 9.5), 40% saturated ammonium sulfate, 0.002 mM FAD, 0.1 mM glutathione, and 1 mM *p*-OHB or 2 mM *p*-ABA. Final small adjustments of the holding solution to the desired pH values were obtained by the addition of concentrated sulfuric acid or ammonium hydroxide. Upon opening the crystallization capillaries, crystals were transferred to holding solutions of the desired pH. After the crystals were mounted, the pH of the holding solution was checked directly in the X-ray capillaries using a microelectrode (Microelectrodes Inc., Londonberry, NH), prior to sealing the capillary before data collection and again at the end of data collection. Excursions of pH during data collection did not exceed 0.06 pH unit for any of the crystals analyzed. All the crystals of the *P. aeruginosa* enzyme (Table 1) were orthorhombic, space group $C222_1$, and isomorphous to those of the *P. fluorescens* enzyme (Schreuder *et al.*, 1988). Since the amino acid sequence of the *P. aeruginosa* enzyme differs from that of the *P. fluorescens* enzyme in only two surface positions (Lah *et al.*, 1994b), the structure of the *P. fluorescens* enzyme was used as the starting model for structure refinement. The initial stage of refinement used only reflections from 5 Å to the resolution limit. Model coordinates were adjusted to each unit cell by treating the three domains of the enzyme, the FAD, and the substrate as rigid bodies using the rigid-body refinement routine of X-PLOR (Brünger, 1992). Positional parameters were then refined with X-PLOR using simulated annealing with the slow-cool protocol (Brünger *et al.*, 1990) from 1000 to 300 K, followed by Powell minimization (Powell, 1977). Thermal parameters were adjusted after each round of refinement of the positional parameters. After addition of water molecules using the program O (Jones *et al.*, 1991), a solvent mask was computed with a probe of 1.4-Å radius and bulk solvent parameters were determined. All independent parameters were refined again, including the reflections in the range 15−5 Å. Alternate conformations present in some of the structures (for example, the two conformations of the segment from Pro293 to Ala296 in the structure of the enzyme in complex with *p*-OHB at pH 9.4) were refined using an iterative procedure that, starting from an initial guess of both the temperature factor and the occupancy of the conformers, involved several cycles in which first the temperature factors and then the occupancies were refined independently until convergence.

The data set collected for the PHBH−*p*-OHB complex at pH 5.0 is of lower quality than that collected for crystals at pH 7.4 (Table 1). To determine if the absence of WAT1 in the structure of the PHBH−*p*-OHB complex at pH 5.0 is a consequence of the lower resolution and lower quality of the data set, the following procedure was adopted. First, the difference temperature factor (ΔB) between the data set at pH 7.4 and the data set at pH 5.0 was determined in the resolution range 15−2.5 Å using the program Scaleit of the CCP4 (Collaborative Computational Project Number 4, 1994) program suite. Best correlation between the two data sets was found by applying an isotropic temperature factor $B = 5.2$ to the pH 7.4 data set that was truncated at 2.5 Å. Improved equivalence between the two data sets was demonstrated by the almost identical values of the spherical averages of intensities calculated for both sets in bins of equal $(\sin^2\theta)/\lambda^2$ in the resolution range 15−2.5 Å. Since this rescaling does not affect the intrinsic quality of the data set, which is higher for pH 7.4 (as indicated by the lower values of R_{sym}, final R, and RMS coordinate error of the refined structure; see Table 1), the pH 7.4 data set was modified to

decrease the accuracy of the observed reflections. This was accomplished by adding a resolution-dependent random error with a Gaussian distribution around the intensity of each reflection. The error for each reflection was calculated according to the function error(H) = gauss[$I(H)S(H)^2K$], where gauss(x) is a gaussian distribution around 0.0 of standard deviation x, H is the index of the reflection, S is the scattering vector, and I is the corrected intensity. K is a resolution-independent constant that was modified by trial and error until rerefinement of the structure of the complex at pH 7.4 against the modified data set resulted in a final R factor ($R = 0.167$) comparable to that of the structure at pH 5.0 ($R = 0.169$) and a RMS coordinate error of 0.31 Å, slightly larger than that of the structure at pH 5.0 (RMS coordinate error = 0.29 Å). This procedure effectively degraded the quality of the pH 7.4 data set so that the structure derived from it could be legitimately compared to the structure at pH 5.0.

Molecular Dynamics. Molecular dynamics simulations were used to determine the most probable orientation of hydrogen bonds in the chain. Since the residues of the chain form an elongated "active site", a modification of the classical dynamics with stochastic boundary conditions (Brooks *et al.*, 1985) was implemented using X-PLOR (Brünger, 1992). Although the enzyme is known to be a dimer in solution, the regions that contribute the elongated active site are not part of the interface between the monomers. Therefore only one monomer was simulated. Two spheres of solvation of 22-Å radius were generated around the ϵ-nitrogen of His72 and the C(7) of the isoalloxazine ring of FAD: the solvation spheres were built by replicating a cubic box of water molecules with a density of 0.0334 molecule Å^{-3} (provided in X-PLOR), generated using the TIPS3P model of water (Jorgensen *et al.*, 1981) and preequilibrated at 300 K by a Monte Carlo procedure. During the generation of the solvation shells, water molecules whose oxygens or hydrogens were less than 2.6 Å from any non-hydrogen atom in the protein or in other preexisting solvent molecules were discarded. All atoms belonging to residues having at least one atom less than 7 Å from any member of the chain (*p*-OHB, Tyr201, Tyr385, Wat2, Wat1, and His72; see Figure 1) were allowed to move in the force field without restraints. The isoalloxazine and ribityl chain atoms of FAD were included in this region, which comprised a total of 1515 atoms. Two additional shells of protein atoms were defined: the first included all the residues having at least one atom less than 4 Å from a residue of the inner sphere of "free" atoms. The remaining atoms of the FAD (including the two phosphates) were selected as part of this shell, which comprised a total of 1610 atoms. The second shell included all the residues having at least one atom less than 3 Å from a residue of the first shell, accounting for a total of 1231 atoms.

The non-hydrogen atoms in the first and second shell were harmonically restrained according to their crystallographic temperature factor B. In this case the restoring force constant k is given by the relationship $k = 3\, k_{\mathrm{Boltzmann}}T/\langle u^2\rangle$, where the atomic mean square displacement $\langle u^2\rangle$ is related to the crystallographic temperature factor B by

$$B = (8/3)(\pi^2\langle u^2\rangle)$$

No restraints were applied to a total of 271 water molecules that were situated within 16 Å from the ϵ-nitrogen of His72 and the C(7) of the isoalloxazine ring of FAD. The oxygens of the 591 waters situated between 16 and 22 Å from the ϵ-nitrogen of His72 and the C(7) of the isoalloxazine ring of FAD were harmonically restrained (force constants of 10 kcal mmol^{-1} Å^{-2}). The remaining atoms of the structure were kept fixed during the simulation. Altogether the simulated system comprised 6942 nonfixed atoms. Nonbonded interactions between the fixed atoms and the "free" or "restrained" atoms were disregarded. Interactions between bonded atoms were computed for all the nonfixed regions and between the nonfixed and the fixed part of the protein. Prior to molecular dynamics the energy of the system was minimized, first freeing the solvent, then the protein, and then solvent and protein simultaneously during the final round of minimization. The RMS difference between the initial crystal structure and the minimized structure used in the simulation was 0.26 Å. Molecular dynamics simulations were carried out with temperature coupling (coupling constant for all atoms = 30 ps^{-1}) according to the method described by Berendsen *et al.* (1984), with Shake restraints (van Gunsteren & Berendsen, 1977) on all bonds. The CHARMM22 force field (Brooks *et al.*, 1983) with explicit polar and nonpolar hydrogens was used. Basic and acidic residues were assigned unit charges; histidines were treated as neutral [H on the ϵ-nitrogen] unless specifically indicated. A step size of 2.5 fs was adopted. After an equilibration ramp in which the temperature of the system was slowly raised from 5 to 300 K over 7.5 ps, the system was further equilibrated for an additional 7.5 ps, after which trajectories were recorded for variable times ranging from a minimum of 25 ps to a maximum of 100 ps. Equilibration of the system, as estimated from the invariance of the atomic displacement correlation functions among consecutive fractions of the recorded simulation, was achieved before the recording of trajectories started. The average temperature and RMS deviation at the end of the simulation were 300 K and 2.2 K.

The radial distribution function G(r) of the hydrogen(s) of hydrogen bond donors was calculated for concentric shells of equal Δr (0.05 Å) around the geometric center of mass of potential hydrogen-bond acceptors. The integral of $G(r)$ was then normalized for the total number of frames in the simulation in order to derive the accumulated probability of finding the hydrogens of a donor within spheres of given radii around the hydrogen-bond acceptor.

Pre-Steady-State Kinetics. Kinetics of the reductive and oxidative reactions were measured by stopped-flow methods using a Hi-Tech stopped-flow apparatus controlled by KISS software (Kinetic Instruments Inc.). Methods of preparation and data analysis were as described previously (Entsch *et al.*, 1991; Palfey *et al.*, 1994).

RESULTS AND DISCUSSION

Structures of PHBH from P. aeruginosa in Complex with p-OHB or p-ABA at pH 5.0, 7.4, and 9.4. We have determined the structure of PHBH from *P. aeruginosa* at three different pH values (5.0, 7.4, and 9.4) for the enzyme in complex with *p*-OHB and with *p*-ABA (Table 1). Since

Table 2: Selected Parameters of PHBH with the Substrate *p*-OHB (or *p*-ABA) in the pH range 6.5−9.5[a]

pH	% hydroxyl of *p*-OHB[b]	k_{red}[c] (s^{-1})	k_{ox}[c] (M^{-1} s^{-1})	k_{hydrox}[c] (s^{-1})	k_{cat}[d] (s^{-1})	K_m *p*-OHB[d] (μM)	k_{cat}/K_m[e] (M^{-1} s^{-1})	K_d *p*-OHB[f] (μM)
6.5	100 (100)	50 (0.091)	2.8×10^5	47(4.9)	12.8	15.8	0.81×10^6	19 (20)
8.0	100	51	3.2×10^5	111	39.0	25.9	1.5×10^6	18 (24)
9.5	76	52	2.6×10^5	50	21.1	240	0.09×10^6	231 (147)

[a] Buffers were potassium phosphate, pH 6.5; Tris sulfate, pH 8.0; and Bis-tris propane sulfate, pH 9.5. Values at pH 6.5 are derived in part from Entsch *et al.* (1976, 1991). Values in parentheses refer to *p*-ABA as substrate and were determined at 25 °C except for k_{hydrox}, which was determined at 4 °C. [b] Hydroxylation stoichiometries were determined at 25 °C in the presence of 247 μM NADPH, 240 μM O_2, and 100 μM *p*-OHB and refer to the percentage of NADPH oxidized that resulted in hydroxylated product. [c] Rate constants for the reduction of FAD by NADPH (k_{red}, step 1 of Scheme 1), the formation of flavin hydroperoxide (k_{ox}, step 2 of Scheme 1), and the disappearance of flavin hydroperoxide (k_{hydrox}, step 3 of Scheme 1; this is equal to the rate of substrate hydroxylation when the hydroxylation stoichiometry is 100%, but if the hydroxylation stoichiometry is less than 100%, then only part of k_{hydrox} represents the rate of substrate hydroxylation) were measured a 4 °C in 50 mM buffer as described previously (Entsch & Ballou, 1989). [d] Turnover numbers and K_m values for *p*-OHB were measured from the initial velocity of NADPH consumption at 25 °C in the presence of 247 μM NADPH, 240 μM O_2, and variable [*p*-OHB], in 50 mM buffer. [e] Apparent k_{cat}/K_m ($\approx k_{on}$) for *p*-OHB with other substrates as in footnote *d*. [f] Dissociation constants for *p*-OHB and *p*-ABA were determined in the presence of 50 mM buffer and 20 μM PHBH by analysis of the spectral changes of the flavin chromophore at 385 nm at 25 °C induced by increasing concentrations of substrate.

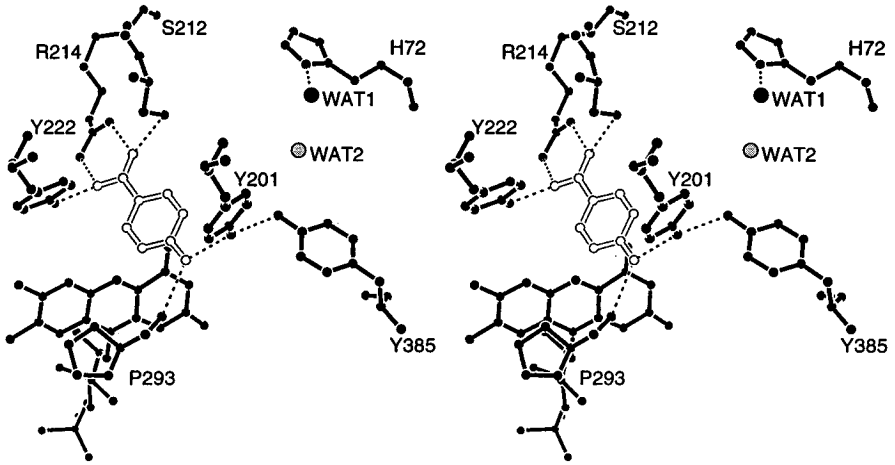

FIGURE 1: Active site of PHBH, shown with the substrate *p*-OHB bound and the *re* side of the flavin facing the viewer. *p*-Hydroxybenzoate occupies a pocket near C(4a) and O(4) of the flavin isoalloxazine ring. Its carboxylate group is stabilized by interactions with the guanidinium of Arg214 and the hydroxyls of Tyr222 and Ser 212. When the hydroxyl of the substrate is not ionized, a hydrogen-bonded chain (dashed) is presumed to connect Tyr385 with the carbonyl oxygen of Pro293. WAT1 (solid circle) is hydrogen-bonded to the δ-nitrogen of His72 and also to the carbonyl oxygen of Gly74 and to the backbone amide of Leu199 (not shown). WAT2 (shaded circle) is visible only in the mutant Y201F in complex with *p*-OHB and in the wild-type enzyme in complex with *p*-ABA. In the presence of WAT2, an extended chain of hydrogen bonds can form, starting with the 4-OH of the substrate, continuing through the hydroxyl groups of Tyr201, Tyr385, and the two water molecules, and ending at the δ-nitrogen of His72. This complete chain of hydrogen bonds would be about 15 Å long.

the 4-OH of bound *p*-OHB has a pK_a between 7.4 and 8.0,[2] it is essentially fully protonated at pH 5.0, partially protonated at pH 7.4, and deprotonated at pH 9.4. In contrast, the 4-amino group of *p*-ABA has two protons throughout the pH range 5.0−9.4. It should be noted, however, that *p*-ABA is a real substrate for the enzyme and that although the amino group is not deprotonated, electron donation from the amino group to the aromatic ring allows the hydroxylation reaction to proceed at a rate that is one-tenth that of *p*-OHB (Entsch *et al.*, 1976; see also Table 2). Therefore, the structures determined for the enzyme in complex with *p*-ABA provide an informative comparison to distinguish the general effects of the solvent pH on the enzyme from the specific structural changes due to protonation/deprotonation of *p*-OHB.

The structure of PHBH in complex with *p*-OHB at pH 7.4 suggests that the substrate hydroxyl group is part of a hydrogen-bonded chain connecting *p*-OHB with Tyr385 (Figure 1). When the hydrogen bonds are oriented in the direction *p*-OHB > Y201 > Y385 (the arrows indicate the direction of the hydrogen bond from donor to acceptor), a proton may be transferred from the substrate to Tyr201; a similar jump would transfer a proton from Tyr201 to Tyr385. However, further proton jumps toward bulk solvent are hindered by the isolation of the Tyr385 hydroxyl from potential hydrogen-bond donors or acceptors. In fact, an elongated cavity separates Tyr385 from His72, a residue located at the surface of the protein and directly exposed to solvent. This cavity is partially filled by a buried water molecule (WAT1, Figure 1) hydrogen-bonded to the δ-nitrogen of His72. In the *P. aeruginosa* enzyme in complex with *p*-OHB, the hydroxyl oxygen of Tyr385 is 5.6 Å from the oxygen of WAT1. As noted by Lah *et al.* (1994a) for the *P. aeruginosa* enzyme and by Schreuder *et al.* (1994) for the *P. fluorescens* enzyme, an uninterrupted chain of hydrogen bonds can be formed transiently between the substrate 4-hydroxyl and His72 through the intercalation of a second water molecule (WAT2, Figure 1) between Tyr385 and WAT1. For instance, the X-ray structure of the mutant enzyme Y201F (Lah *et al.*, 1994a,b) shows a strong electron density peak, representing a solvent molecule that occupies the gap between Tyr385 and WAT1. This extra water is even more prominent in the structure of the wild-type enzyme

[2] A value of 7.4 has been reported in previous studies (Entsch *et al.*, 1991). Re-evaluation with improved correction for unbound *p*-OHB in the optical determination of the ionization state of bound *p*-OHB provides a value close to 8.0.

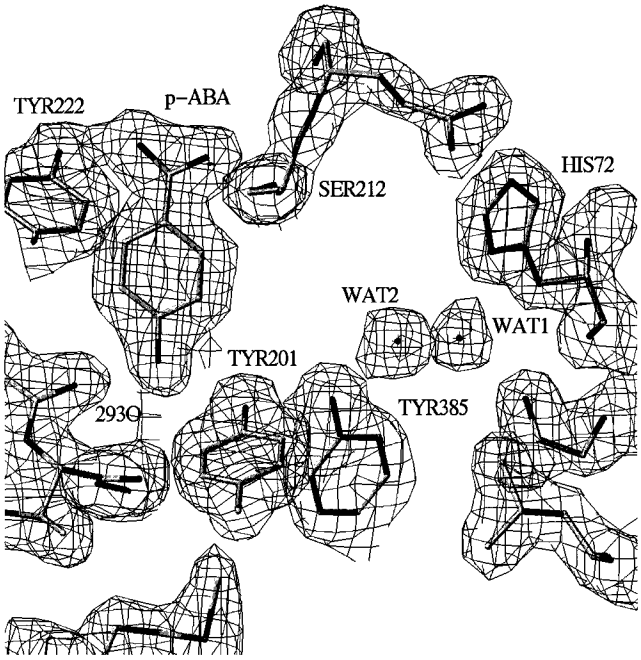

FIGURE 2: Residues and water molecules that form a chain of hydrogen bonds between the substrate and His72 in PHBH in complex with *p*-ABA at pH 7.4. A $|2F_o - F_c|$ map of the enzyme is contoured at 1.0σ. Electron density corresponding to WAT1 and WAT2 is clearly visible.

crystallized in the presence of *p*-ABA at pH 7.4 (Figure 2). Refinement of positional and thermal parameters has confirmed the presence of the extra water in both structures.

In the case of *p*-ABA in complex with PHBH, the orientation of the hydrogen-bonds in the chain can be deduced from the chemical properties of the ligand. Since the amino group of *p*-ABA has two protons, it is expected to act as hydrogen bond donor to both the carbonyl of Pro293 and the hydroxyl of Tyr201. In this complex Tyr201 would donate a hydrogen bond to Tyr385, which in turn would be a donor to the neighboring water (WAT2 of Figure 2). In the mutant Y201F, where WAT2 is also clearly visible, the absence of the hydroxyl oxygen of Tyr201 as a possible acceptor appears to favor donation of a hydrogen bond from Tyr385 to WAT2, thus stabilizing WAT2. This event is even more likely to occur when the substrate donates a hydrogen bond to Tyr201, forcing this residue to serve as a donor to Tyr385.

The structure of PHBH in complex with *p*-OHB at pH 5.0 shows changes in the density corresponding to His72, suggesting that the imidazole ring has undergone a rotation around the β-γ bond (compare Figure 3, panels a and c). The average temperature factor of the His72 side chain at pH 5.0 ($\langle B \rangle = 39.5$) (Table 3) is much higher than the corresponding value at pH 7.4 ($\langle B \rangle = 18.3$) or at pH 9.4 ($\langle B \rangle = 15.4$), indicating that the imidazole ring is not well-ordered at pH 5.0. The structure at pH 5.0 provides additional insights concerning interactions that stabilize WAT1 and WAT2 in their respective pockets. At this pH neither WAT1 nor WAT2 is visible when *p*-OHB is bound in the active site (Figure 3b). The interpretation of these findings is in principle complicated by the lower quality and lower resolution (2.5 Å, Table 1) of the pH 5.0 data set with respect to the pH 7.4 data set, which may make the detection of WAT1 and WAT2 problematic at pH 5.0. Indeed, examination of Table 1 reveals that the structure of the *p*OHB complex at pH 5.0 has fewer solvent molecules (146 *versus* 231) than the structure at pH 7.4. To address this problem we repeated the refinement of the pH 7.4 structure using a data set that was truncated at 2.5 Å and artificially degraded by the addition of a resolution-dependent random error (see Materials and Methods). After modification of the data set, fewer solvent molecules (169 *versus* 231) with temperature factors less than 60 Å^2 could be identified in the electron density map. Comparisons of maps based on the pH 5.0 data set and on the modified pH 7.4 data set are shown in Figure 3. WAT1 is not visible in the electron density map derived from the pH 5.0 data set even when the density is contoured at 0.2σ (panel b) or lower δ. In contrast, WAT1 is readily visible at higher levels of electron density (0.7σ) in the map derived from the modified pH 7.4 data set (panel c). Also visible is the different orientation of the His72 imidazole ring at pH 5.0 (panels a and b) and at pH 7.4 (panel c).

Altogether these structural changes are suggestive of different ionization states of His72 at pH 5.0 (protonated) and pH 7.4 (neutral). The absence of WAT1 at pH 5.0 suggests that this water is stabilized at pH 7.4 by donating a hydrogen bond to a neutral His72. The rotation of the His72 side chain at pH 5.0 probably contributes to the loss of WAT1. The absence of WAT2 at both pH 7.4 and 5.0 indicates that when the 4-hydroxyl of *p*-OHB is protonated, it donates a hydrogen bond to Pro293 rather than to Tyr201.

When *p*-ABA is bound in the active site, WAT1 and WAT2 are both visible at pH 5.0 (Figure 4). WAT2 is presumably stabilized by the hydrogen-bonding network from *p*-ABA to Tyr201 to Tyr385 to WAT2. The His72 side chain is also better defined than when *p*-OHB is bound, and its average temperature factor is only slightly higher than its value at pH 7.4 ($B = 21.3$ at pH 5.0 *versus* $B = 14.8$ at pH 7.4) (Table 3). A possible interpretation of this finding is that the pK_a of His72 is modulated by the direction of hydrogen bonds in the chain and is lower with *p*-ABA bound than with *p*-OHB. The density of WAT1 is less defined at pH 5.0 (Figure 4) than the equivalent density present in the structure at pH 7.4, and the temperature factor of its oxygen is significantly higher ($B = 30.2$ versus $B = 13.7$ at pH 7.4) (Table 3). This indicates that the hydrogen bond formed between WAT1 and WAT2 compensates only partially for the decreased interaction between WAT1 and a protonated (or partially protonated) His72.

The analysis of PHBH with *p*-OHB bound at pH 9.4 reveals important structural changes in the vicinity of the substrate. The carbonyl of Pro293 is now 3.2 Å from the O4 of *p*-OHB, *versus* 2.8 Å at pH 5.0 and 7.4 (Table 4).[3] The segment from Pro293 to Ala296 [the loop joining strand D3 to helix H10 (Schreuder *et al.*, 1988)] adopts two conformations, with the largest differences occurring in the peptide bond between Thr294 and Gly295 (Figure 5). The structure was refined with both conformations present. The temperature factors and relative occupancy of the conformers were refined iteratively until a difference map computed with

[3] Analysis of the difference distance matrix (Nishikawa *et al.*, 1972) between the structure at pH 7.4 and the structure at pH 9.4 indicates that the increase in the distance between the substrate hydroxyl and the carbonyl of Pro293 observed at pH 9.4 is due to a motion of the latter group, and not of the substrate, with respect to the other atoms in the structure.

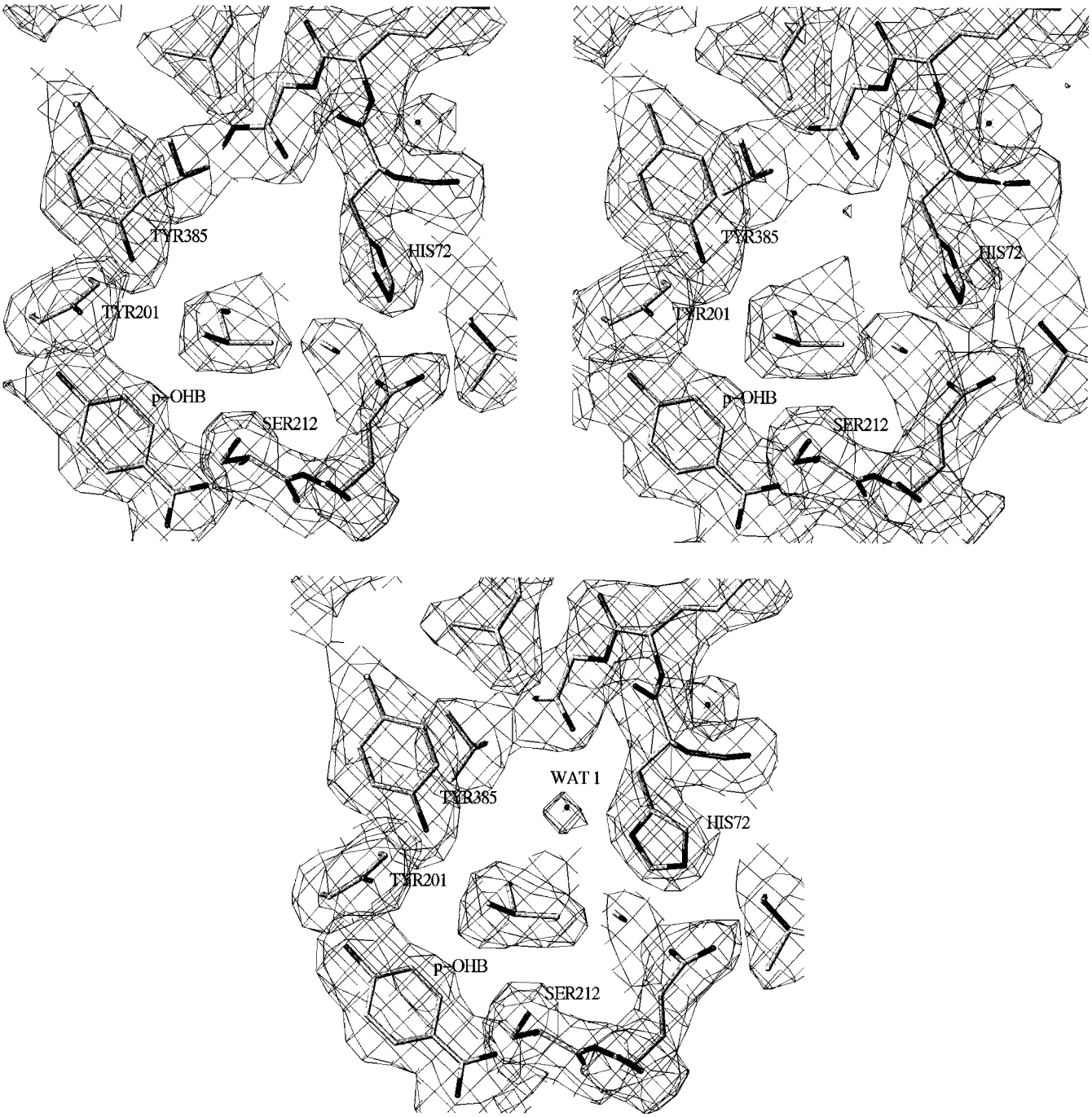

FIGURE 3: (Panel a, top left) Structural changes in PHBH with bound *p*-OHB at pH 5.0. A view of the groups involved in the formation of the chain of hydrogen bonds is presented from a different angle than in Figures 1 and 2. The model of PHBH at pH 5.0 is shown with oxygen and nitrogen atoms represented by darker shades of gray. A $|2F_o - F_c|$ SA-omit map of the enzyme at pH 5.0 is contoured at 0.7σ. The side chain of His72 was omitted from this refinement, and weighted coefficients for the Fourier synthesis were derived with Sigmaa (Read, 1986). (Panel b, top right) Same map as in panel a, but contoured at 0.2σ to show that WAT 1 is not visible even at low levels of electron density. (Panel c, bottom) Electron density of the enzyme in complex with *p*-OHB at pH 7.4 obtained with a data set truncated at 2.5 Å and degraded by the addition of a resolution-dependent random error (see Materials and Methods). A $|2F_o - F_c|$ SA-omit map of the enzyme is contoured at 0.7σ. WAT1 and the side chain of His72 were omitted from this refinement and weighted coefficients for the Fourier synthesis were derived with Sigmaa (Read, 1986).

coefficients $|F_o - F_c|$ did not show residual density in the region. The new orientation of the peptide, rotated by almost 180° with respect to the conformation observed at pH 5.0 and 7.4, brings the amide -NH of Gly295 within hydrogen-bonding distance (3.3 Å) of O(4) of *p*-OHB. In this alternate conformation a hydrogen bond is formed between the carbonyl of Thr294 and a solvent molecule (WAT of Figure 5). These changes are consistent with the presence of a repulsive interaction between the deprotonated substrate and the carbonyl of Pro293 (Table 4) and the formation of a new hydrogen bond between the substrate $O(4)^-$ and Gly295-NH.

The structure of PHBH with *p*-ABA bound at pH 9.4 is almost identical to the structure at pH 7.4 and does not show the structural changes that are observed in the vicinity of the substrate when *p*-OHB is bound (Figure 6). This is expected, since *p*-ABA has the same ionization state at pH 7.4 and at 9.4. Thus, it can be argued that the changes

Table 3: Average Temperature Factors (Å^2) of Selected Residues in the Structures of PHBH in Complex with *p*-OHB and *p*-ABA at pH 5.0, 7.4, and 9.4[a]

	p-OHB			*p*-ABA		
	5.0	7.4	9.4	5.0	7.4	9.4
$\langle B_{side} \rangle$[a]	27.7 ± 19.3	24.3 ± 15.1	22.0 ± 14.9	24.5 ± 16.6	24.4 ± 14.1	22.4 ± 14.4
substrate	15.3	11.8	10.5	11.6	10.0	10.5
Pro293	10.6	11.4	12.7	13.6	12.2	11.0
Tyr201	10.0	11.2	8.1	10.3	10.0	10.5
Tyr385	16.1	15.2	13.0	14.5	12.9	13.2
Wat2				14.1	7.9	14.7
Wat1		18.7	14.3	30.2	13.7	19.0
His72	39.5	18.3	15.4	21.3	14.8	15.1

[a] Average temperature factor of side-chain atoms ± RMS deviation.

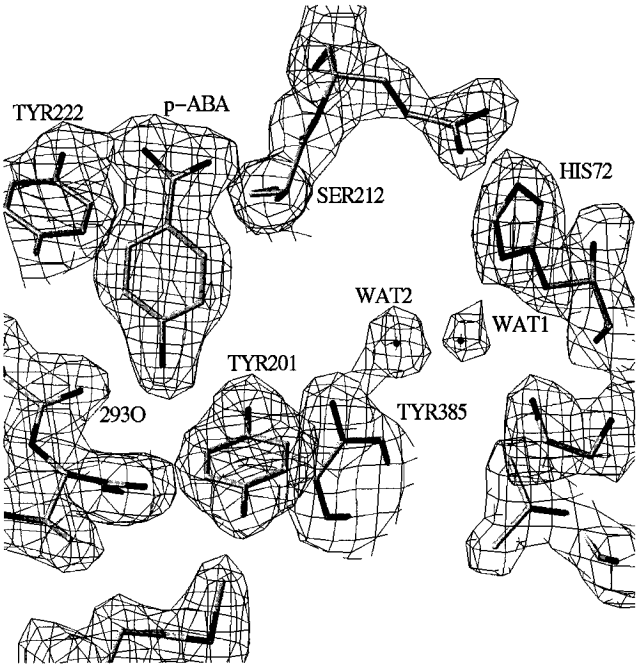

FIGURE 4: Residues and solvent molecules involved in the formation of the chain of hydrogen bonds in PHBH in complex with *p*-ABA at pH 5.0. A $|2F_o - F_c|$ map of the enzyme is contoured at 1.0σ. Electron density corresponding to WAT1 and WAT2 is visible. Note, however, the smaller density of WAT1 with respect to structure at pH 7.4 (Figure 2).

observed with *p*-OHB bound, when going from pH 7.4 to 9.4, are due primarily to deprotonation of the substrate. A similar increase in the K_d values for both *p*-OHB and *p*-ABA is observed at pH 9.5 with respect to pH 8.0 (Table 2). However, the structure of the enzyme in complex with *p*-ABA does not reveal significant changes between pH 7.4 and 9.4 in the hydrogen-bond coordination of the substrate (Table 4). Therefore, other factors, like the ionization state of the substrate-free enzyme, are likely to contribute a large fraction of the difference in the binding energy of the two substrates between pH 8.0 and 9.5.

Geometric Requirements for Proton Transfer. In the crystalline enzyme−*p*-OHB complex, protonated *p*-OHB is likely to be hydrogen-bonded to the carbonyl of Pro293 (*vide supra)*. In fact, WAT2 is observed only when *p*-ABA binds in the active site and, by virtue of the two protons on the amino group, donates one hydrogen bond to Pro293 and one hydrogen bond to Tyr201. This produces an orientation of hydrogen bonds between *p*-ABA, Tyr201, and Tyr385 opposite to that observed when *p*-OHB is bound. However, transient reorientation of the hydroxyl of *p*-OHB is expected

Table 4: Distances (Å) between Selected Atoms in the Structures of PHBH in Complex with *p*-OHB and *p*-ABA at pH 5.0, 7.4, and 9.4

	p-OHB			*p*-ABA		
	5.0	7.4	9.4	5.0	7.4	9.4
sub[a] O1*−Arg214 NH1	2.68	2.83	2.83	2.82	2.85	2.84
sub O2*−Arg214 NH2	2.79	2.81	2.84	2.89	2.87	2.89
sub O1*−Tyr222 OH	2.58	2.62	2.61	2.69	2.62	2.68
sub O2*−Ser212 OG	2.77	2.70	2.67	2.76	2.76	2.76
sub O4/N4−Pro293 O	2.85	2.83	3.26[b] 3.11[c]	2.97	3.02	3.06
sub O4/N4−Tyr201 OH	2.61	2.80	2.69	3.03	3.07	3.06
Tyr201 OH−Tyr385 OH	2.79	2.85	2.68	2.88	2.89	2.91
Tyr385 OH−Wat2 O				2.73	2.64	2.74
Wat2 O−Wat1 O				2.85	2.79	2.81
Wat1 O−His72 ND1		2.76	2.72	2.72	2.72	2.67

[a] Substrate: *p*-OHB or *p*-ABA. [b] Conformation of the loop 293−296 with the carbonyl of Thr294 closer to the substrate O(4). [c] Conformation of the loop 293−296 with the amide of Gly 295 closer to the substrate O(4).

to produce a situation similar to that induced by *p*-ABA; in this case the *p*-OHB hydroxyl would donate a hydrogen bond to Tyr201, resulting in stabilization of WAT2 (*vide infra*). Protonation/deprotonation of *p*-OHB or a reaction intermediate could then take place *via* proton jumps along the chain of hydrogen bonds completed by WAT2 (Nagle & Morowitz, 1978; Schulten & Schulten, 1986). Orientation of the hydrogen bonds in the chain in the direction of His72 or in the direction of the substrate would determine whether protons are extracted from the active site or channeled into it.

We have used molecular dynamics simulations to study the conditions that control the directions of the hydrogen bonds in the chain. A time average of the pattern of hydrogen-bond formation during the simulation was derived from the radial distributions of the hydrogen(s) of hydrogen-bond donors (D) around potential acceptors. The integral of the radial distribution around acceptor A of the hydrogen belonging to D−H, normalized for the total number of frames in the simulation, provides the probability of finding the hydrogen of D−H inside a sphere of a given radius around A. If the two species form a hydrogen bond, the probability of finding the hydrogen of D−H will start increasing when the radius of the sphere about A is ≥ 1.5 Å (corresponding to a strong hydrogen bond) and should reach unity for radii ≥ 2.5 Å. For a species with two donor hydrogens (water, for example), the probability of finding a hydrogen will reach a maximum value of 2 (1 for each hydrogen). In the case of a single acceptor near HOH, the probability of finding a donor hydrogen is expected to reach unity inside a sphere

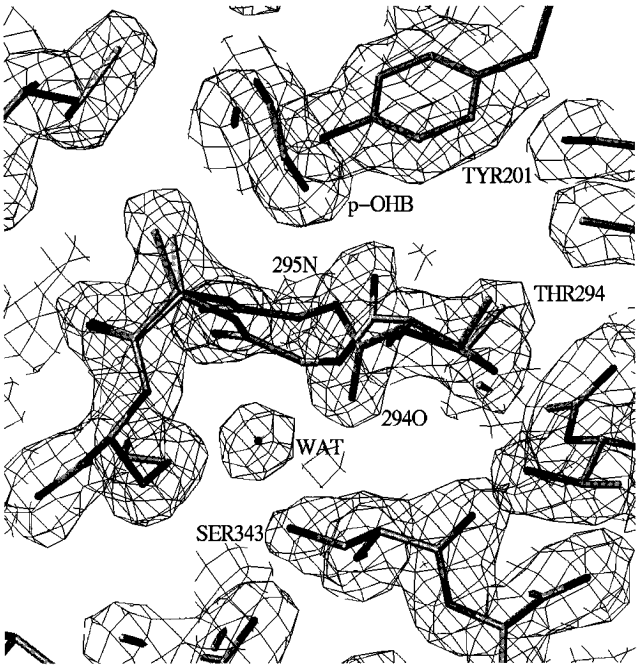

FIGURE 5: Structural features near *p*-OHB at pH 9.4. The model of PHBH is shown with two conformations of the loop from Pro293 to Ala296 (oxygen and nitrogen atoms are represented with darker shades of gray). The labels 294O and 295N identify the carbonyl oxygen of Thr294 and the amide nitrogen of Gly295 in the alternate conformation of the loop visible at pH 9.4 but not at pH 7.4. A SA-Sigmaa weighted (Read, 1986) omit map of the region (residues 294 and 295 were omitted from the model during refinement) computed with coefficients $|2F_o - F_c|$ is shown contoured at 1σ.

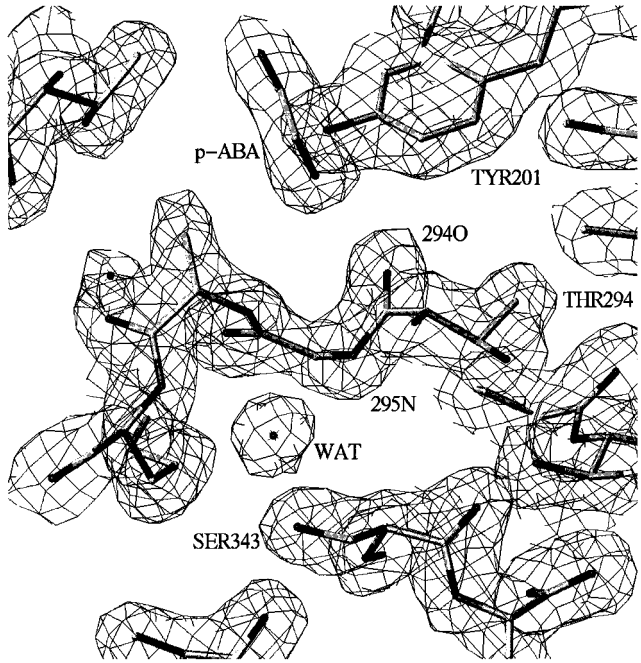

FIGURE 6: Structural features near *p*-ABA at pH 9.4. A map of the same region shown in Figure 5 was computed with coefficients $|2F_o - F_c|$ and is contoured at 1σ. Only one conformation of the backbone of the loop Pro293−Ala296 is present.

of 2.5 Å around the acceptor, while the probability of finding the second hydrogen will reach unity only inside spheres of larger radii, which are not compatible with the formation of a hydrogen bond (see Figure 7).

First we were interested in determining whether a simulation would confirm the intuitive assignment of the hydrogen-bond orientation in the enzyme complexed with *p*-ABA. The assignment, based on crystallographic observations and the chemical properties of *p*-ABA (see above), provides a useful benchmark for testing the behavior of the enzyme during molecular dynamics simulations. Simulation of the enzyme with *p*-ABA bound and the δ-nitrogen of His72 deprotonated produced a configuration with hydrogen bonds propagating in the direction

p-ABA > Y201 > Y385 > WAT2 > WAT1 > H72

where > indicates the direction of the hydrogen bond from donor to acceptor (data not shown).

As a second step we have attempted to simulate conditions that are not readily amenable to crystal structure analysis. WAT2 is never observed in the crystals in the presence of *p*-OHB, but as discussed above, it might be transiently stabilized in the pocket between Tyr385 and WAT1 when *p*-OHB is a hydrogen-bond donor to Tyr201. What would then be the orientation of hydrogen bonds in the chain when WAT2 coexists with *p*-OHB? In order to answer this question we added WAT2 to the system in the simulation of the enzyme with bound *p*-OHB and studied several combinations of protonation states of both the substrate and His72, which are the two end groups of the full chain of hydrogen bonds.

The average orientation of hydrogen bonds during the simulation of the enzyme in complex with protonated *p*-OHB (with the δ-nitrogen of His72 deprotonated), can be derived from the columns of Figure 7 that are labeled pOHB(H):H72. In these columns all the combinations of hydrogen bonds that might occur between potential donors and acceptors are considered. In the leftmost column we look for the hydrogen bonds directed from His72 toward the substrate. In this column the panel labeled Y201(H)-pOHB-(O4) shows that the hydrogen of the Tyr201 hydroxyl is situated more than 3 Å from the substrate O(4) and therefore does not form a hydrogen bond to the substrate. Similarly, the panel labeled Y385(H)−Y201(O) shows that Tyr385 does not donate a hydrogen bond to Tyr201. The panel labeled WAT2(H*)-Y385(O) shows that both hydrogens of WAT2 are beyond hydrogen-bonding distance (∼3.3 Å) of the Tyr385 hydroxyl, and the panel labeled WAT1(H*)−WAT2-(O) shows that neither hydrogen of WAT1 forms a hydrogen bond with the oxygen of WAT2. In the third column from the left we look for the hydrogen bonds directed from the substrate toward His72. The top three panels of this column show that the hydrogen of *p*-OHB hydrogen-bonds to the oxygen of Tyr201, the hydrogen of Tyr201 hydrogen-bonds to the oxygen of Tyr385, and the hydrogen of Tyr385 hydrogen-bonds to the oxygen of WAT2. In the fourth panel, labeled WAT2(H*)−WAT1(O), it is shown that one hydrogen of WAT2 is within hydrogen-bonding distance of the oxygen of WAT1 (∼2.2 Å) and the other one is not (∼3.1 Å). In the fifth panel, labeled WAT1(H*)−H72(N), one hydrogen of WAT1 is within hydrogen-bonding distance (∼2.1 Å) of the δ-nitrogen of His72 and the other one is not (∼3.3 Å).

Altogether, these results indicate that when *p*-OHB is protonated and His72 is deprotonated, hydrogen-bond donation propagates in the direction

p−OHB > Y201 > Y385 > WAT2 > WAT1 > H72

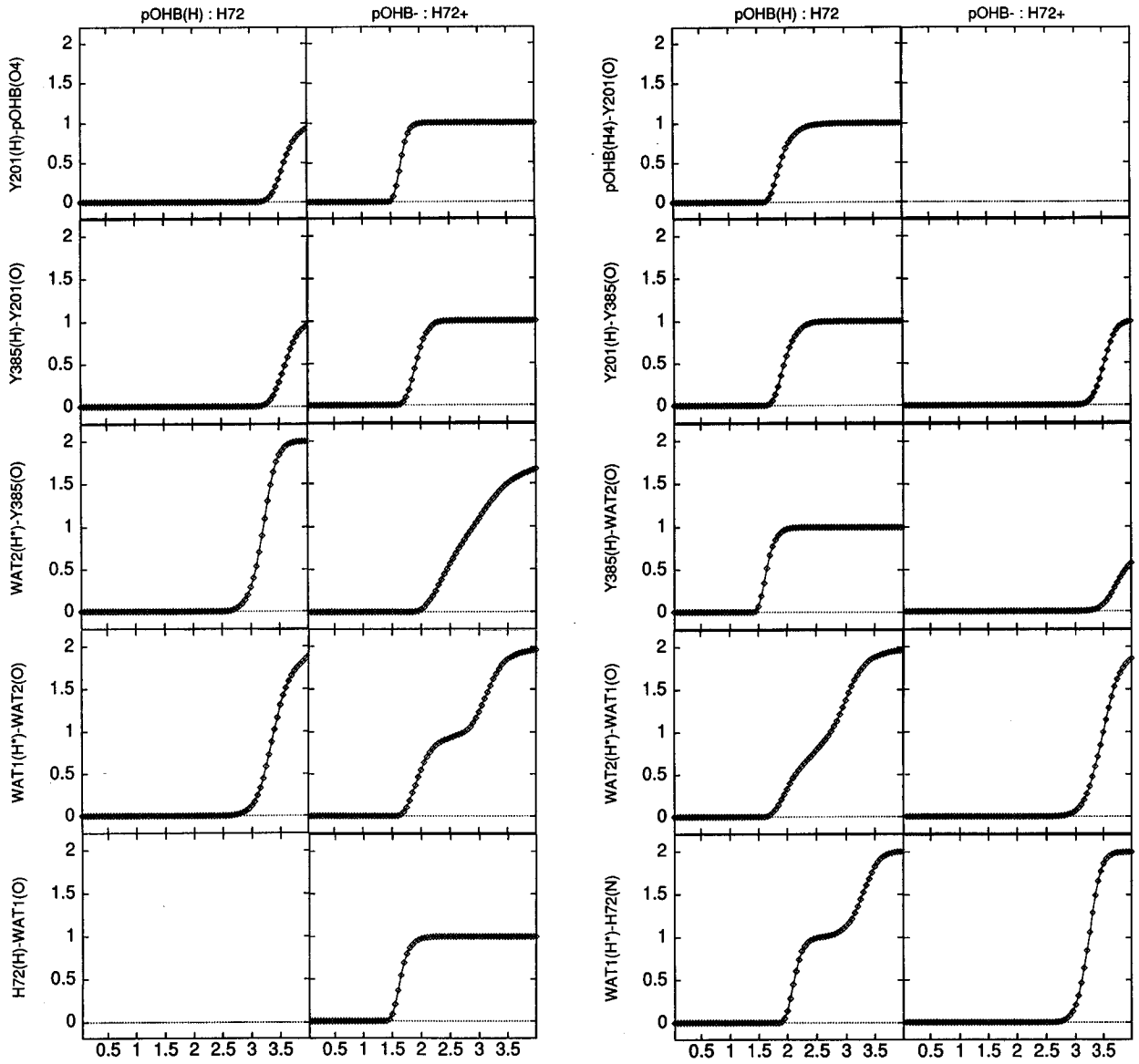

FIGURE 7: Panels from top to bottom in the first and second columns from the left show, respectively, the radial distributions of (1) the hydrogen of Tyr201 around the substrate O(4) [row labeled Y201(H)−pOHB(O4)], (2) the hydrogen of Tyr385 around the hydroxyl oxygen of Tyr201 [row labeled Y385(H)−Y201(O)], (3) the hydrogens of WAT2 around the hydroxyl oxygen of Tyr385 [row labeled WAT2-(H*)−Y385(O)], (4) the hydrogens of WAT1 around the oxygen of WAT2 [row labeled WAT1(H*)−WAT2(O)], and (5) the hydrogen of the δ-nitrogen of His72 [row labeled H72(H)−WAT1(O)]. Panels from top to bottom in the third and fourth columns from the left show, respectively, the radial distributions of (1) the hydrogen of the substrate around the hydroxyl oxygen of Tyr201 [row labeled pOHB(H4)−Y201(O)], (2) the hydrogen of Tyr201 around the hydroxyl oxygen of Tyr385 [row labeled Y201(H)−Y385(O)], (3) the hydrogen of Tyr385 around the oxygen of WAT2 [row labeled Y385(H)−WAT2(O)], (4) the hydrogens of WAT2 around the oxygen of WAT1 [row labeled WAT2(H*)−WAT1(O)], and (5) the hydrogens of WAT1 around the δ-nitrogen of His72 [row labeled WAT1(H*)−H72(N)]. These radial distributions were determined from molecular dynamics simulations of the enzyme with His72 protonated in complex with deprotonated *p*-OHB (columns labeled pOHB−:H72+) or of enzyme with His72 deprotonated in complex with protonated *p*-OHB [columns labeled pOHB(H):H72]. The probability of finding the hydrogen(s) of a hydrogen-bond donor (1 for the tyrosine hydroxyl hydrogen and 2 for the water hydrogens) inside spheres of a given radius around the hydrogen-bond acceptor is shown on the ordinate *versus* the sphere radius (angstroms). A distribution of the donor hydrogen between 1.4 and 2.5 Å from the acceptor indicates formation of a hydrogen bond.

This average configuration of the chain of hydrogen bonds was observed during the simulation for a continuous period of approximately 20 ps. Another configuration was observed in the next 80 ps of the simulation, in which the pattern of hydrogen-bond donation was

P293 < *p*-OHB < Y201 > Y385 > WAT2 > WAT1 > H72

where the arrows on both sides of Tyr201 indicate that this residue is donating a hydrogen bond with approximately equal probability to either the substrate or Tyr385. This simulation shows the ability of the hydroxyl groups of substrate and tyrosine to rotate about the C−O axis.

During the simulation of the enzyme in complex with deprotonated *p*-OHB and protonated His72, hydrogen-bond donation was oriented in the direction

H72 > WAT1 > WAT2 > Y385 > Y201 > *p*-OHB

as indicated in Figure 7, columns labeled $pOHB^{-}$:$H72^{+}$. The interpretation of these traces is similar to that described for the columns labeled pOHB(H):H72. In a simulation of the enzyme with both the substrate and His72 deprotonated,

Scheme 3: Proton Relay Mechanisms in PHBH[a]

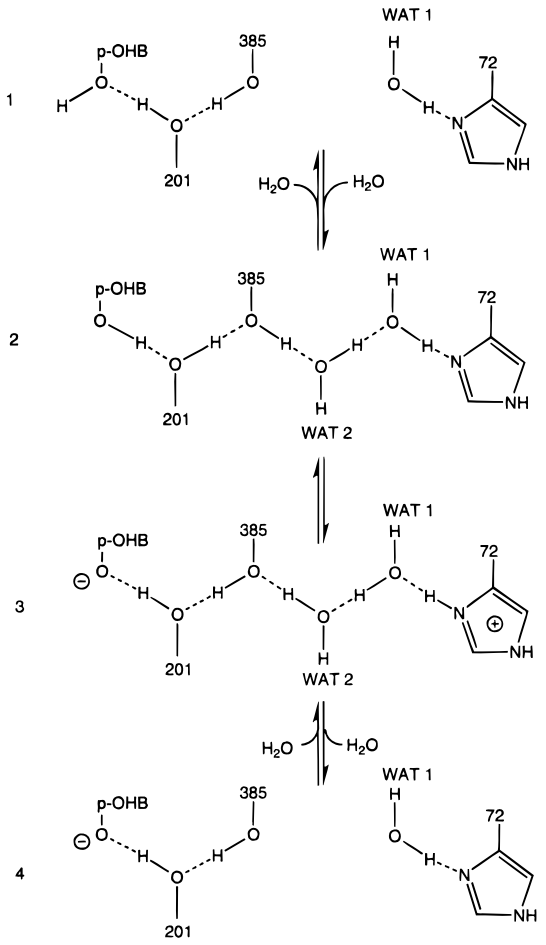

WAT2 abandoned its pocket near WAT1 during the equilibration time, and during the following observation time of 20 ps WAT2 occupied a new position in which it receives a hydrogen bond from Tyr385 but has no hydrogen bond to WAT1. Thus, hydrogen-bond donation was oriented in the direction

$$p\text{-OHB} < \text{Y201} < \text{Y385} \gg \text{WAT2 (gap) WAT1} > \text{H72}$$

where the double arrow on the right side of Tyr385 indicates that this residue donates a hydrogen bond with higher probability to WAT2 than to Tyr201.

In conclusion, the simulations show that the simultaneous presence of protonated substrate and deprotonated His72 can polarize the chain of hydrogen bonds toward His72. Polarization in the opposite direction is observed when *p*-OHB is deprotonated and His72 is protonated. These configurations, shown as states 2 and 3 in Scheme 3, may partially represent transition states in the process of proton translocation along the chain of hydrogen bonds. In Scheme 3, the state arising immediately after the substrate binds is labeled 1. In state 2 it is envisioned that a rotation of the hydroxyl groups of the substrate, Tyr201 and Tyr385, would favor the entry of a water molecule (WAT2) and would produce a transient polarization of the chain of hydrogen bonds in the direction of His72, as observed during the simulation with protonated substrate and neutral His72. This configuration may favor deprotonation of the substrate and induce a change of proton coordination throughout the chain as shown in state 3. The orientation of hydrogen bonds ensuing after proton transfer (state 3) is consistent with the simulation of the enzyme with deprotonated substrate and positive His72 (Figure 7). The protonated His72 (which at physiological pH is above its pK_a) could then release the proton to the solvent. This might be aided by a rotation of His72, consistent with the high temperature factor of this residue observed in the crystal structure of the enzyme with bound *p*-OHB at pH 5.0 (also see Figure 3). The structure at pH 5.0, which shows the effects produced by stable protonation of His72, provides insights into the effects of transient protonation of this residue during turnover. In the final configuration (state 4), obtained after His72 releases a proton to the solvent and the substrate is deprotonated, WAT2 is not stabilized and is therefore lost.

MECHANISTIC CONCLUSIONS

Scheme 3 diagrams intermediate conformations in which the enzyme may promote proton transfer to and from the active site. All the steps leading to substrate deprotonation can be easily reversed in order to return a proton to the reaction intermediate to form product. The structures of the enzyme in complex with *p*-OHB and *p*-ABA show that Tyr201 and Tyr385 can donate hydrogen bonds in either of two orientations: in the direction of either the substrate (structures with *p*-OHB) or His72 (structures with *p*-ABA). Reorientation is accomplished through a rotation of the tyrosine hydroxyls (Schulten & Schulten, 1986; Zundel, 1986). The structure of the enzyme in complex with *p*-OHB at pH 5.0 shows that the imidazole ring of His72 is mobile when protonated and may undergo rotation around the β-γ bond. The two water molecules that complete the chain of hydrogen bonds are also mobile: molecular dynamics simulations show that both water molecules can easily change orientation depending on the protonation state of the substrate or of His72. Thus, all the groups involved in the formation of the chain of hydrogen bonds can undergo orientation changes. Rotation of ionizable groups has been postulated to be an important step in the process of translocating protons inside proteins (Nagle & Morowitz, 1978; Schulten & Schulten, 1986), since the rotation of a side group such as Tyr will transport a proton by approximately 2 Å. Further motion of a proton requires a jump to a different carrier, a step of length 0.5−1.5 Å. Deprotonation of *p*-OHB is thus envisioned as a proton jump to the neighboring Tyr201. It does not require that a particular proton be transferred over the long distance (>15 Å) that separates the substrate hydroxyl from solvent. States 2 and 3 described in Scheme 3 can be imagined to be in equilibrium, permitting protons to be shifted to and from the intermediates in catalysis.[4]

A critical feature of the proposed proton transfer scheme is the presence of WAT2. The simulations, the structure with the substrate *p*-ABA, and the structure of *p*-OHB in

[4] From molecular dynamics trajectories it is possible to follow hydrogen−acceptor geometry as a function of time. For each frame of the simulation a goodness of fit criterion *G*(H) for the existence of a hydrogen bond was defined, and an index for the coexistence of multiple hydrogen bonds in the chain was derived as the product of the *G*(H) values of individual hydrogen bonds. This analysis indicated that the frequency at which all the hydrogen bonds in the chain are oriented in the direction of the deprotonated substrate (when His72 is protonated) or in the direction of His72 (when this residue is neutral and the substrate *p*-OHB is protonated) is of the order of $\sim 10^{11}$ s^{-1}. Therefore, the rate of proton release or uptake by the chain may be governed by other factors, including the relative p*K*s of the chain components and the rate of exchange of Wat2.

complex with the mutant Y201F (Lah *et al.*, 1994a,b) all demonstrate that WAT2 is stabilized by receiving a hydrogen bond from Tyr385. For the wild-type enzyme in complex with the substrate *p*-OHB, formation of the transient species (2 or 3) incorporating WAT2 may therefore be relatively rare events.

The structure of the enzyme in complex with *p*-OHB at pH 9.4 suggests a possible mechanism by which the orientation of the hydrogen bonds in the chain is altered, as in interchange of states 2 and 3 of Scheme 2. In this structure, where the substrate is expected to be completely deprotonated, the backbone of the loop from Pro293 to Ala296 is present in two conformations (Figure 5). During turnover, transition of the protein from a state similar to that observed at pH 7.4 to a state similar to that observed at pH 9.4, or *vice versa*, could then favor deprotonation or protonation of intermediates.

A pH-dependent peptide flip similar to that found in PHBH has been observed in the analyses of oxidized *P. aeruginosa* azurin at pH 5.5 and 9.0 (Nar *et al.*, 1991). In this case the conformational transition was attributed to protonation/deprotonation of a histidine close to the copper binding site. The pK_a of this histidine is 6.2 in the Cu(II) protein and 7.2 in the reduced Cu(I) form (Hill & Smith, 1976, 1979). Thus, in azurin, changes emanating from the copper binding site affect the pK_a of a nearby histidine and link protonation to electron transfer. The conformational transition observed in PHBH could likewise be dependent on the chemical properties of the intermediate flavin species. For example, formation of the flavin hydroperoxide could favor the conformation of the peptide associated with deprotonation of the substrate. However, no conformational changes appear to be associated with reduction of the flavin *per se*, as evidenced by the high-resolution structure of the reduced form of PHBH (Schreuder *et al.*, 1992), which at pH 7.4 is virtually identical to the oxidized form.

The importance of the chain of hydrogen bonds in the hydroxylation reaction is supported by the effects of mutations in some of its key residues. The hydroxylation rate is decreased by a factor of 1000 in the mutant Y201F and by a factor of 50 in the mutant Y385F (Entsch *et al.*, 1991; Eschrich *et al.*, 1993). The elimination of the hydroxyl of Tyr201 has the most devastating effect because this group is likely to be the immediate acceptor of a proton from the substrate as well as the donor to the reaction intermediate (Scheme 2b). The studies reported here emphasize that the binding and mobility of water molecules may contribute significantly to the rate at which proton transfer reactions take place.

ACKNOWLEDGMENT

We thank Dr. B. A. Palfey for contributing comments and ideas to the development of this project; Dr. H. J. C. Berendsen, Dr. S. Krimm, and Dr. W. H. Dunham for suggestions and comments regarding the molecular dynamics simulations; and Dr. B. A. Palfey and Ms. M. Ortiz Maldanado for crystallizing PHBH and providing purified enzyme for kinetic studies. The drawings of atomic models of Figure 1 were prepared by Anita Metzger using the program MAXIM written by Mark Rould. The drawings of atomic model and electron densities of Figures 2−6 were prepared using the program O (Jones *et al.*, 1991).

REFERENCES

Berendsen, H. J. C., Postma, J. P. M., van Gunsteren, N. F., DiNola, A., & Haak, J. R. (1984) *J. Chem. Phys. 81*, 3684−3690.

Brooks, B. R., Bruccoleri, R. E., Olafson, B. D., States, D. J., Swaminathan, S., & Karplus, M. (1983) *J. Comput. Chem. 4*, 187−217.

Brooks, C. L., Brunger, A., & Karplus, M. (1985) *Biopolymers 24*, 843−865.

Brunger, A. (1992) *X-PLOR, Version 3.1*, (Yale University, New Haven, CT.

Brunger, A. T., Krukowski, A., & Erickson, J. (1990) *Acta Crystallogr. A46*, 585−593.

Collaborative Computational Project Number 4 (1994) *Acta Crystallogr. D50*, 760−763.

Entsch, B., & Ballou, D. P. (1989) *Biochim. Biophys. Acta 999*, 313−322.

Entsch, B., Ballou, D. P., & Massey, V. (1976) *J. Biol. Chem. 251*, 2550−2563.

Entsch, B., Palfey, B. A., Ballou, D. P., & Massey, V. (1991) *J. Biol. Chem. 266*, 17341−17349.

Eschrich, K., van der Bolt, F. J. T., de Kok, A., & van Berkel, W. J. H. (1993) *Eur. J. Biochem. 216*, 137−146.

Gatti, D., Palfey, B. A., Lah, M. S., Entsch, B., Massey, V., Ballou, D. P., & Ludwig, M. L. (1994) *Science 266*, 110−114.

Hill, H. A. O., & Smith, B. E. (1976) *Biochem. Biophys. Res. Commun. 70*, 331−338.

Hill, H. A. O., & Smith, B. E. (1979) *J. Inorg. Biochem. 11*, 79−93.

Jones, T. A., Zou, J. Y., Cowan, S. W., & Kjeldgaard, M. (1991) *Acta Crystallogr. A47*, 110−119.

Jorgensen, W. L., Chandraseckhar, J., Madura, J. D., Impey, R. W., & Klein, M. L. (1983) *J. Chem. Phys. 79*, 926−935.

Lah, M. S., Gatti, D., Schreuder, H. A., Palfey, B. A., & Ludwig, M. L. (1994) in *Flavins and Flavoproteins 1993*, (Yagi, K., Ed.) pp 221−229, Walter de Gruyter, Berlin.

Lah, M. S., Palfey, B. A., Schreuder, H. A., & Ludwig, M. L. (1994b) *Biochemistry 33*, 1555−1564.

Nagle, J. F., & Morowitz, H. J. (1978) *Proc. Natl. Acad. Sci. U.S.A. 75*, 298−302.

Nar, H., Messerschmidt, A., Huber, R., van de Kamp, M., & Canters, G. (1991) *J. Mol. Biol. 221*, 765−772.

Nishikawa, K., Ooi, T., Isogai, Y., & Saito, N. (1972) *J. Phys. Soc. (Japan) 32*, 1331−1337.

Palfey, B. A. (1993) Ph.D. Dissertation, The University of Michigan, Ann Arbor, MI.

Palfey, B. A., Entsch, B., Ballou, D. P., & Massey, V. (1994) *Biochemistry 33*, 1545−1554.

Powell, M. J. D. (1977) *Math. Program. 12*, 241−254.

Read, R. J. (1986) *Acta Crystallogr. A42*, 140−149.

Schreuder, H. A., van der Laan, J. M., Hol, W. G. J., & Drenth, J. (1988) *J. Mol. Biol. 199*, 637−648.

Schreuder, H. A., Hol, W. G. J., & Drenth, J. (1990) *Biochemistry 29*, 3101−3108.

Schreuder, H. A., van der Laan, J. M., Swarte, M. B. A., Kalk, K. H., Hol, W. G. J., & Drenth, J. (1992) *Proteins: Struct., Funct., Genet. 14*, 178−190.

Schreuder, H. A., Mattevi, A., Obmolova, G., Kalk, K. H., Hol, W., van der Bolt, F. J. T., & van Berkel, W. J. H. (1994) *Biochemistry 33*, 10161−10170.

Schulten, Z., & Schulten, K. (1986) *Methods Enzymol. 127*, 419−438.

Shoun, H., Higashi, N., Beppu, T., & Arima, K. (1974) *FEBS Lett. 49*, 13−17.

Shoun, H., Beppu, T., & Arima, K. (1979) *J. Biol. Chem. 254*, 899−904.

van Berkel, W. J. H., & Muller, F. (1989) *Eur. J. Biochem. 179*, 307−314.

van der Laan, J. M., Swarte, M. B. A., Groendijk, H., Hol, W. G. J., & Drenth, J. (1989) *Eur. J. Biochem. 179*, 715−724.

van Gunsteren, W. F., & Berendsen, H. J. C. (1977) *Mol. Phys. 34*, 1311−1315.

Vervoort, J., Rietjens, M. C. M., van Berkel, J. H., & Veeger (1992) *Eur. J. Biochem. 206*, 479−484.

Wessiak, A., Schopfer, L. M., & Massey, V. (1984) *J. Biol. Chem. 259*, 12547−12556.

Zundel, G. (1986) *Methods Enzymol. 127*, 439−455.

BI951344I